

Channel thickness optimization for ultra thin and 2D chemically doped TFETs

Chin-Yi Chen, Tarek A. Ameen, Hesameddin Ilatikhameneh, Rajib Rahman, Gerhard Klimeck, Joerg Appenzeller

Abstract—2D material based tunnel FETs are among the most promising candidates for low power electronics applications, since they offer ultimate gate control and high current drives that are achievable through small tunneling distances (Λ) during the device operation. The ideal device is characterized by a minimized Λ . However, devices with the thinnest possible body do not necessarily provide the best performance. For example, reducing the channel thickness (T_{ch}) increases the depletion width in the source which can be a significant part of the total Λ . Hence, it is important to determine the optimum T_{ch} for each channel material individually. In this work, we study the optimum T_{ch} for three channel materials: WSe₂, Black Phosphorus (BP), and InAs using full-band self-consistent quantum transport simulations. To identify the ideal T_{ch} for each material at a specific doping density, a new analytic model is proposed and benchmarked against the numerical simulations.

Index Terms—tunnel transistors, channel thickness, quantum transport.

I. INTRODUCTION

The supply voltage of metal oxide semiconductor field-effect transistors (MOSFETs) has almost stopped scaling since the beginning of the millennium, since the sub-threshold swings in conventional transistors cannot be improved beyond 60 mV/dec at room-temperature for fundamental reasons. Even today's state-of-the-art 14nm tri-gate MOSFET does not operate below 0.6V [1]. For decades, the semiconductor industry has been researching transistors with steeper subthreshold characteristics $I_D - V_G$ than obtainable in conventional FETs with the goal to enable low supply voltages to reduce power consumption [2], [3]. Unlike MOSFETs, tunneling field effect transistors (TFETs) are not bound by the 60mV/dec limit and

This work was supported in part by the Center for Low Energy Systems Technology (LEAST), one of six centers of STARnet, a Semiconductor Research Corporation program sponsored by MARCO and DARPA.

The authors are with the Department of Electrical and Computer Engineering, Purdue University, West Lafayette, IN, 47907 USA e-mail: chen1648@purdue.edu

can operate at significantly lower voltages [4]–[7]. Such merit makes TFETs an appealing alternative option to MOSFETs for low power applications [8], [9]. However, TFETs utilize band to band tunneling (BTBT) to switch the device ON and OFF, and the BTBT process limits the ON current (I_{ON}) accordingly.

I_{ON} is proportional to the BTBT transmission probability (T_{BTBT}) which can be expressed in terms of both electrostatics and material properties [11] as

$$I_{ON} \propto T_{BTBT} \propto e^{-\Lambda \sqrt{m^* E_g}}, \quad (1)$$

where in the simplest picture m^* is the reduced effective mass along the transport direction ($\frac{1}{m^*} = \frac{1}{m_x^*} + \frac{1}{m_y^*}$). E_g is the band gap of the channel material and Λ is the tunneling distance at the junction. Reducing $\Lambda \sqrt{m^* E_g}$ increases T_{BTBT} and I_{ON} exponentially. For a more detailed discussion on equation (1) and its accuracy, please refer to Appendix I.

For a chemically doped TFET, the total tunneling distance (Λ) has two contributions [10], [11]: the depletion width (W_D) in the doped source region and the scaling length (λ) in the channel as shown in Fig. 1.

Reducing the channel thickness (T_{ch}) is beneficial in terms of electrostatics and may translate into a smaller Λ [9] if for example W_D does not depend on T_{ch} . In reality, however, W_D is thickness dependent in a low dimensional system (i.e. 2D material). This has been demonstrated experimentally [12], numerically, and analytically [12]–[15] where W_D is larger in a 2D compared to a 3D PN junction. In a 2D PN junction, W_D is inversely proportional to the thickness [13].

$$W_D = \frac{\pi \epsilon \Delta V}{q N T_{ch}} \quad (2)$$

where N is the doping density and ΔV is the built-in potential. ϵ is an averaged dielectric constant of the channel material and the dielectric surrounding the source. λ for a chemically doped

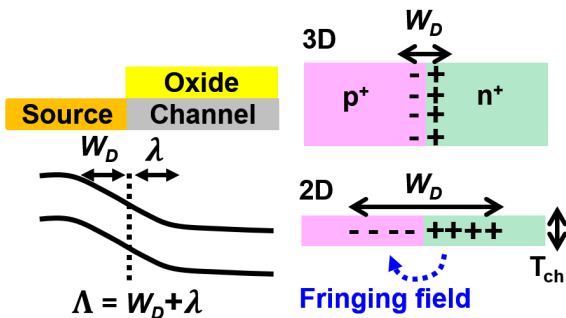


Fig. 1: TFET's tunneling distance (Λ) contains a depletion width (W_D) in the source region and the scaling length (λ) in the channel. W_D of the 2D PN junction is larger than W_D of the 3D PN junction due to the presence of fringing fields.

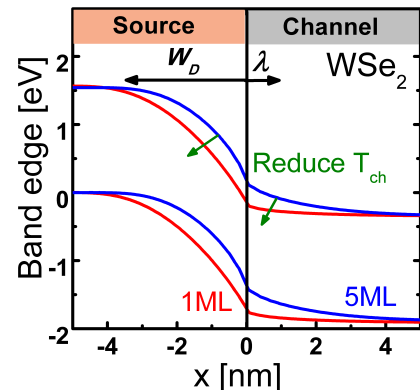


Fig. 2: Band diagrams of a mono-layer and a 5ML WSe₂ TFET extracted from atomistic quantum transport simulations.

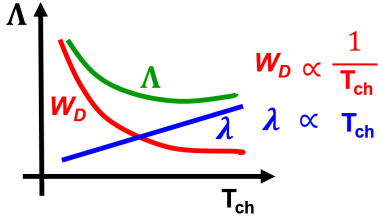


Fig. 3: Scaling length (λ) is proportional to T_{ch} while depletion width (W_D) is inversely proportional to T_{ch} . As a result, the thinnest possible T_{ch} does not guarantee the smallest Λ .

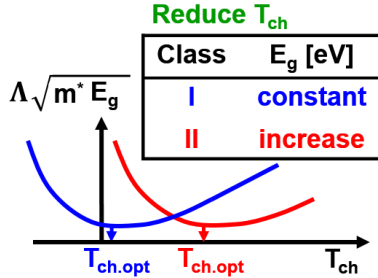


Fig. 4: An optimum channel thickness ($T_{ch,opt}$) exists that minimizes $\Lambda\sqrt{m^*E_g}$. Depending on whether or not E_g changes with the channel thickness (T_{ch}), the optimum body thickness ($T_{ch,opt}$) occurs at smaller or larger T_{ch} respectively.

double gated 2D TFET [16] can be approximated as

$$\lambda = \frac{\varepsilon}{\varepsilon_{ox}} [\gamma_1 T_{ch} + \gamma_2 T_{ox}] \quad (3)$$

where ε_{ox} and T_{ox} are the dielectric constant and the thickness of the gate oxide in Fig. 1, respectively. γ_1 and γ_2 are fitting parameters, since the expression without γ_1 and γ_2 was derived for an electrostatically doped 2D TFET [16], [17].

Fig. 2 shows that λ and W_D respond to T_{ch} in the opposite fashion as illustrated in the band diagrams extracted from atomistic simulations of a mono-layer (1ML) and a 5ML WSe₂ TFETs. When T_{ch} is reduced from 5ML to 1ML, λ is reduced due to the tighter gate control according to eq. (3) while W_D increases according to eq. (2). As a result, the thinnest possible T_{ch} may not minimize Λ as shown in Fig. 3.

Moreover, the channel thickness (T_{ch}) that minimizes the total tunneling distance (Λ) is not necessarily the best T_{ch} overall since material parameters might change also with T_{ch} . To obtain the highest I_{ON} , the optimum T_{ch} should minimize the entire expression $\Lambda\sqrt{m^*E_g}$. In this work, a compact model to optimize T_{ch} for the ON state ($T_{ch,opt}$) is introduced, and the model is benchmarked with state-of-the-art atomistic quantum transport simulations.

Materials considered in this article can be classified depending on how their band gap changes with T_{ch} . We define class I materials as those that do not show a dependence of E_g on T_{ch} , which, as will be discussed below, results in thinner $T_{ch,opt}$ for optimum ON-state performance. On the other hand, class II materials, according to our definition, exhibit a decrease of E_g with increasing T_{ch} . As a result, an optimum design is achieved with a relatively thicker $T_{ch,opt}$. Details are described later.

In sections II and III, the impact of the body thickness on material properties and tunneling distance are discussed. Section IV shows the optimized T_{ch} for the ON-state obtained from an analytic analysis and atomistic quantum transport

simulations. Section V shows the upper limit of T_{ch} in a TFET. Last, section VI summarizes the T_{ch} design rules for a TFET.

II. THE IMPACT OF T_{ch} ON E_g AND m^*

Three channel materials are considered in this work: WSe₂, BP, and InAs. BP and InAs are chosen, because their small direct E_g occurs promising for TFET applications [18]–[21]. Note that in the case of InAs, body thicknesses beyond what has been experimentally achieved were considered, and that in general transport in channels with T_{ch} below 5 nm is strongly impacted by surface scattering [22], [23], while our model assumes that ballistic transport conditions prevail. WSe₂ is chosen as a case study, since its direct band gap (E_g) barely changes with T_{ch} . Moreover, WSe₂ based TFETs are expected to show the best performance among semiconducting transition metal dichalcogenides (TMDs) [24]–[26].

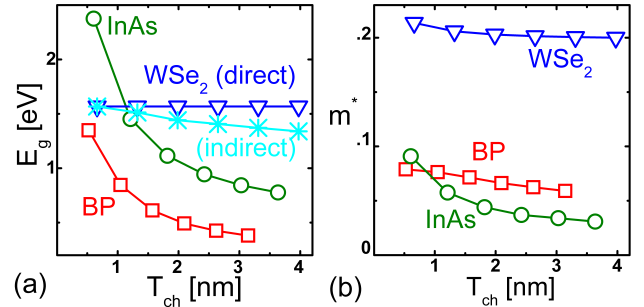


Fig. 5: (a) and (b) show three studied channel materials' E_g and tunneling mass m^* as a function of T_{ch} extracted from atomistic tight binding simulations, which are calibrated against density function theory (DFT).

Fig. 5 shows E_g and tunneling mass m^* of WSe₂, BP, and InAs extracted from atomistic tight binding simulations. The Slater-Koster tight binding parameters [27] of WSe₂ are extracted from the band structure calculated by density function theory (DFT) with generalized gradient approximation (GGA) [24], [28]. Note that E_g is not exactly the same as in some transport experiments [29], but is comparable.

E_g and m^* typically increase with stronger confinement achieved by reducing T_{ch} . The dependence of E_g and m^* on T_{ch} can be expressed as $E_g = E_{g,bulk} + \frac{\alpha}{T_{ch}}$ and $m^* = m_{bulk}^* + \frac{\alpha'}{T_{ch}}$. α and α' are determined from Fig. 5 by fitting. The parameter α for the case of WSe₂ is significantly smaller than in the case of BP and InAs due to weak inter-layer coupling [30], [31].

channel	$E_{g,bulk}$ [eV]	α [eV/nm]	m_{bulk}^* [m_0]	α' [m_0/nm]
WSe ₂	1.535	0.02	0.2	0.01
BP	0.28	0.52	0.055	0.02
InAs	0.35	1.5	0.025	0.035

TABLE I: Parameters $E_{g,bulk}$, m_{bulk}^* , α , and α' for WSe₂, BP, and InAs.

III. THE IMPACT OF T_{ch} ON THE TUNNELING DISTANCE

WSe₂, BP, and InAs 2D TFETs' λ , W_D , and Λ are shown in Fig. 6 (a), (b), and (c). The source doping density (N) is 10^{20} cm^{-3} . All simulated materials show that λ is proportional

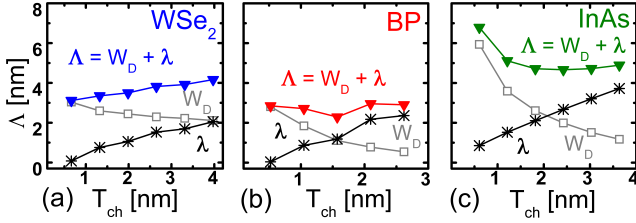


Fig. 6: (a), (b), and (c) Dependence of Λ , λ , and W_D on T_{ch} for WSe₂, BP, and InAs TFETs, respectively.

to T_{ch} while W_D is inversely proportional to T_{ch} . The data are extracted from atomistic quantum transport simulations. The details of the simulation method and the simulated structure is described in Appendix II. W_D in the ON-state is proportional to the potential drop (ΔV) across the depletion layer in the source, which is of the order of E_g . Since E_g of BP and InAs has a stronger dependence on T_{ch} compared to WSe₂, their W_D also shows a stronger dependence on T_{ch} .

IV. THE OPTIMUM T_{ch} FOR ON-STATE ($T_{ch,opt}$)

The optimum T_{ch} ($T_{ch,opt}$) for the ON-state minimizes $\Lambda\sqrt{m^*E_g}$ and is expected to maximize I_{ON} . The dependence of Λ , m^* , and E_g on T_{ch} has been discussed in section II and III. All of them can be expressed as a function of T_{ch} . As a

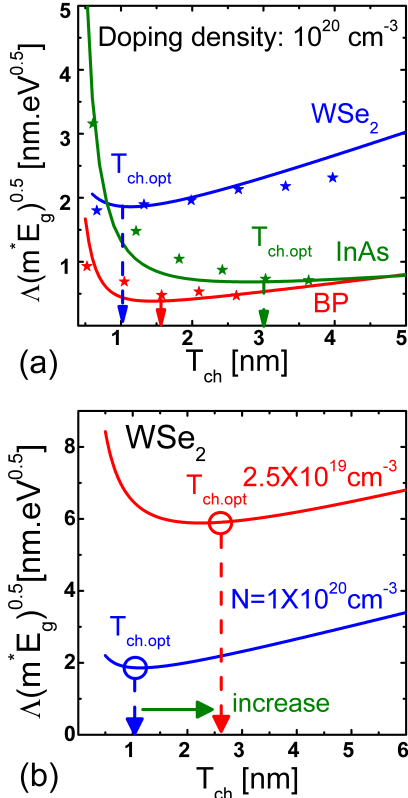


Fig. 7: (a) $\Lambda\sqrt{m^*E_g}$ for WSe₂, BP, and InAs TFETs at a source doping density of 10^{20} cm^{-3} . The solid lines are calculated from eq. (4) with parameters $c_0 \sim c_5$ as listed in Appendix III. The stars are extracted from atomistic quantum transport simulations. (b) $\Lambda\sqrt{m^*E_g}$ of WSe₂ TFETs for two different source doping densities calculated from eq. (4). $T_{ch,opt}$ increases as the doping density is reduced.

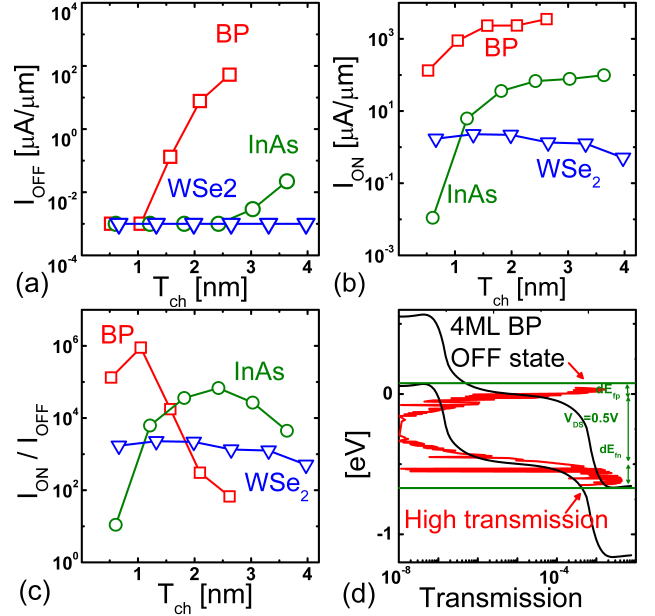


Fig. 8: (a), (b), and (c) Dependence of I_{OFF} , I_{ON} , and the ON/OFF current ratio on T_{ch} . (d) OFF-state transmission for a BP 4ML TFET. A significant source to drain leakage in thick T_{ch} BP (and InAs) TFETs is due to the small E_g .

result, $\Lambda\sqrt{m^*E_g}$ can also be expressed as a function of T_{ch} and is given by

$$\begin{aligned} \Lambda\sqrt{m^*E_g} &= (\lambda + W_D)\sqrt{m^*E_g} \\ &= \left(c_0 T_{ch} + c_1 + c_2 \frac{1}{T_{ch}} + c_3 \frac{1}{T_{ch}^2} \right) c_4 \sqrt{1 + c_5 \frac{1}{T_{ch}}} \end{aligned} \quad (4)$$

parameters $c_0 \sim c_5$ are described in Appendix III in detail. Finding $T_{ch,opt}$ that minimizes $\Lambda\sqrt{m^*E_g}$ can be accomplished analytically or numerically. An exact analytic $T_{ch,opt}$ solved by $\frac{d\Lambda\sqrt{m^*E_g}}{dT_{ch}} = 0$ is complicated to interpret. Therefore, we will focus in the following on the numerical results by calculating $\Lambda\sqrt{m^*E_g}$ at different T_{ch} and find $T_{ch,opt}$ as the minimum of those plots. Fig. 7 (a) shows $\Lambda\sqrt{m^*E_g}$ for WSe₂, BP, and InAs TFETs calculated from eq. (4), corresponding well with the results from atomistic quantum simulations.

It is apparent that WSe₂ as a class I material exhibits a smaller $T_{ch,opt}$ as mentioned before, since $\frac{\alpha}{E_{g,bulk}} \ll 0.5$ nm which is a single atomic layer's thickness. For a class II material like BP or InAs, $\frac{\alpha}{E_{g,bulk}}$ is larger than a mono-layer's thickness which implies a larger $T_{ch,opt}$. Moreover, $T_{ch,opt}$ increases when the source doping density (N) decreases as apparent from fig. 7(b), since W_D inversely proportionally depends on N as stated above.

	WSe ₂	BP	InAs
$\alpha/E_{g,bulk}$ [nm]	0.01	1.8	4.3
Class	I	II	II

TABLE II: Classification of WSe₂, BP, and InAs.

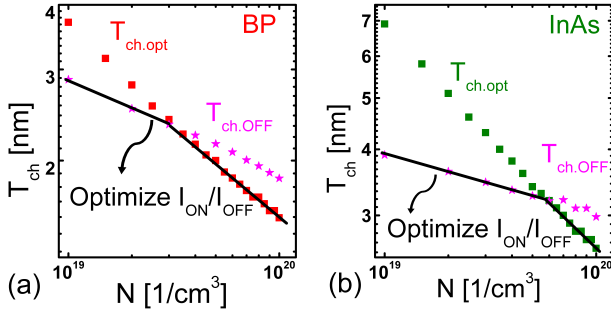


Fig. 9: (a) and (b) $T_{ch,opt}$ and $T_{ch,OFF}$ for different source doping densities. The channel thickness that optimizes the ON/OFF current ratio is $T_{ch,opt}$ or $T_{ch,OFF}$ whichever is smaller; $\min(T_{ch,opt}, T_{ch,OFF})$. Note that $T_{ch,OFF}$ is obtained from atomistic quantum transport simulations for $V_{DS}=0.5V$.

V. AN UPPER LIMIT OF T_{ch} DEFINED BY THE OFF-STATE ($T_{ch,OFF}$)

A thicker channel with a smaller bandgap may increase I_{OFF} and deteriorate the ON/OFF current ratio. An upper limit on T_{ch} can be deduced by considering the maximum permissible OFF current (I_{OFF}). Fig. 8(a), (b), and (c) show the I_{OFF} , I_{ON} , and ON/OFF current ratio extracted from the $I_D - V_G$ curves as calculated from atomistic quantum transport simulations. The simulated structure is shown in Appendix II and assumes the supply voltage (V_{DD}) is 0.5V. The $I_D - V_G$ is shifted by adjusting the OFF-state ($I_D = I_{OFF}$) to $V_G = 0$ V. I_{ON} is extracted at $V_G = V_D = 0.5$ V after shifting the $I_D - V_G$ curves. Following the convention of the ITRS roadmap [2], I_{OFF} is chosen to be $10^{-3} \mu A/\mu m$ or the minimum possible current above this value. I_{OFF} for BP and InAs is substantial when T_{ch} is above 1 nm and 3 nm respectively. This is because E_g in this case is too small to block the tunneling current in the OFF-state as shown in the Fig. 8(d).

The ON/OFF current ratio suffers from significant degradation if the device cannot be turned off effectively as shown in Fig. 8(c). This would occur if $E_g < qV_{DS} + dE_{fp} + dE_{fn}$. dE_{fp} and dE_{fn} are the difference between the Fermi level and the band edge in the degenerately doped source and drain region respectively. There exist a $T_{ch,OFF}$ below which E_g is large enough to suppress the OFF current. Given that, $E_g = E_{g,bulk} + \frac{\alpha}{T_{ch}}$, $T_{ch,OFF}$ can be expressed as

$$T_{ch,OFF} < \left| \frac{\alpha}{qV_{DS} - E_{g,bulk} + dE_{fp} + dE_{fn}} \right| \quad (5)$$

dE_{fn} and dE_{fp} reduces as the doping density decreases, which results in a larger $T_{ch,OFF}$.

To optimize a TFET's ON/OFF current ratio, $T_{ch,opt}$ or $T_{ch,OFF}$ whichever is smaller should be used. Fig. 9 (a) and (b) show how $T_{ch,opt}$ and $T_{ch,OFF}$ for BP and InAs change as a function of the source doping density. Both $T_{ch,opt}$ and $T_{ch,OFF}$ increase as the source doping density is reduced.

VI. SUMMARY

Optimizing the channel thickness of a 2D TFET can significantly improve its performance. The choice of the channel thickness affects both the material properties and the electrostatics. There exists a channel thickness that minimizes the

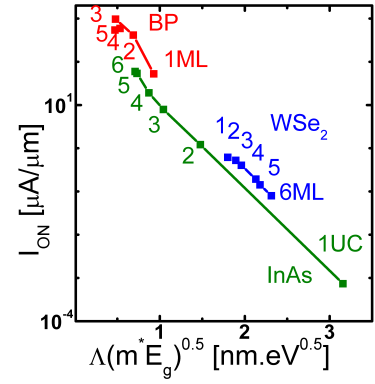


Fig. 10: I_{ON} and its corresponding $\Lambda\sqrt{m^*E_g}$ are extracted from atomistic simulations. I_{ON} is proportional to $e^{-\Lambda\sqrt{m^*E_g}}$. ML and UC are the abbreviations for mono-layer and unit cell respectively.

tunneling distance. However, the ON-state channel thickness ($T_{ch,opt}$) should optimize the product of the band gap, reduced effective mass and square of the tunneling distance. Moreover, a maximum permissible channel thickness ($T_{ch,OFF}$) is needed to reach acceptable OFF-currents. In this work, compact models were introduced to describe these two important channel thicknesses. A 2D TFET exhibits the highest ON/OFF current ratio when the channel thickness is chosen to be the smaller of $T_{ch,opt}$ and $T_{ch,OFF}$.

Appendix I. How descriptive is $I_{ON} \propto e^{-\Lambda\sqrt{m^*E_g}}$?

Knowing how descriptive is $I_{ON} \propto e^{-\Lambda\sqrt{m^*E_g}}$ compared to sophisticated quantum transport simulations is critical before optimizing T_{ch} by minimizing $\Lambda\sqrt{m^*E_g}$. Fig. 10 shows I_{ON} and its corresponding $\Lambda\sqrt{m^*E_g}$ from full band self consistent atomistic simulations.

This compact equation quantitatively represents the trend of sophisticated atomistic simulations, although it assumes a simple potential distribution and a simple m^* [11], Different materials that have the same $\Lambda\sqrt{m^*E_g}$ are expected to provide I_{ON} within the same order of magnitude. However, we find minor deviations between different materials because this compact equation approximates complex band structures by a single band reduced effective mass and ignores contributions from higher sub-bands. To demonstrate the descriptiveness of this compact equation, I_{on} and Λ in Fig. 10 are extracted when the tunneling window is opened to 0.35 eV to reduce contributions from higher sub-bands.

Appendix II. Simulation Details

A schematic structure of the simulated double gated chemically doped TFET is shown in Fig. 11. The channel is 15 nm

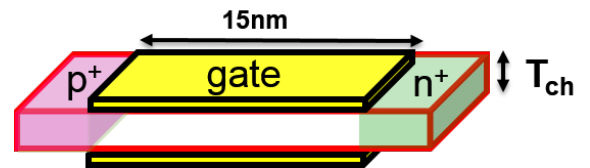


Fig. 11: Structure of the chemically doped TFETs.

with the supply voltage ($V_{DD} = 0.5V$) following the ITRS 15nm technology node [32]. The oxide is assumed to be H_FO_2 with an EOT of 0.5 nm. The source is heavily doped at density $\sim 10^{20} 1/cm^3$.

The numerical simulations are performed self-consistently by coupling quantum trasmissing boundary method (QTBM) and 3D-Poisson equation [33]. 3D finite-difference method is used to calculate the carrier density (ρ). The anisotropic dielectric constant is taken into account in the Poisson equation as shown in eq. (6) [34], [35].

$$\frac{d}{dx} \left(\varepsilon_{in} \frac{dV}{dx} \right) + \frac{d}{dy} \left(\varepsilon_{in} \frac{dV}{dy} \right) + \frac{d}{dz} \left(\varepsilon_{out} \frac{dV}{dz} \right) = -\rho \quad (6)$$

where ε_{in} and ε_{out} are the in-plane and out-of-plane dielectric constants. The QTBM method is equivalent to the nonequilibrium Green's function approach without scattering but is more computationally efficient [24]. The open boundary Schrödinger equation is solved in the following form:

$$(EI - H - \Sigma)\psi = S \quad (7)$$

where E , I , H , and Σ are energy, identity matrix, device Hamiltonian, and the total self-energy due to the open boundaries condition. ψ and S are the wave function in the device and the strength of the carrier injection from contacts respectively. The Hamiltonian is constructed with the second nearest neighbor tight binding method. The simulation is performed by the Nanoelectronics Modeling tool: NEMO5. [36], [37] More simulation details can be found in [20] and [38].

Appendix III Analytical expression for $\Lambda\sqrt{m^*E_g}$

$\Lambda\sqrt{m^*E_g}$ can be expressed as a function of T_{ch} as

$$\Lambda\sqrt{m^*E_g} = (\lambda + W_D)\sqrt{m^*E_g} \quad (8)$$

$$= \left(c_0T_{ch} + c_1 + c_2\frac{1}{T_{ch}} + c_3\frac{1}{T_{ch}^2} \right) c_4\sqrt{1 + c_5\frac{1}{T_{ch}}} \quad (9)$$

where c_0 through $\sim c_5$ are obtained after expressing λ , W_D , m^* , and E_g as a function of T_{ch} . The dependence of m^* and E_g on T_{ch} has been discussed in Section II.

W_D for a 2D PN-junction is given by

$$W_D = \frac{\pi\varepsilon\Delta V}{\ln(4)qNT_{ch}} \quad (10)$$

$$\sim \frac{\pi\varepsilon E_g}{\ln(4)qNT_{ch}} \quad (11)$$

$$\sim \frac{\pi(\varepsilon_1T_{ch} + \varepsilon_2) \left(E_{g,bulk} + \frac{\alpha}{T_{ch}} \right)}{\ln(4)qNT_{ch}} \quad (12)$$

which can be expressed as a function of T_{ch} explicitly. ΔV is of the order of E_g which can be expressed as $E_g = E_{g,bulk} + \frac{\alpha}{T_{ch}}$. ε increases with T_{ch} due to changes in the electrostatic environment and can be expressed as $\varepsilon \sim \varepsilon_1T_{ch} + \varepsilon_2$. ε_1 and ε_2 can be obtained by fitting W_D shown in Fig. 6(a), (b), and (c).

On the other hand, the chemically doped TFET's scaling

channel	ε_1	ε_2
	[ε_0]	[ε_0/nm]
WSe ₂	0.43	0.99
BP	0.62	0.91
InAs	0.83	1.28

TABLE III: Parameters ε_1 and ε_2 for WSe₂, BP, and InAs. $\varepsilon_0 = 8.854 \times 10^{-12} C/(V.m)$.

length (λ) is given by

$$\lambda = \frac{\varepsilon}{\pi\varepsilon_{ox}} [\gamma_1T_{ch} + \gamma_2T_{ox}] \quad (13)$$

$$= L_1T_{ch} + L_2. \quad (14)$$

which is a modified version of the electrically doped TFETs' λ [16], [17]. L_1 and L_2 can be obtained by fitting λ shown in Fig. 6 (a), (b), and (c).

channel	L_1	L_2
	[cons.]	[nm]
WSe ₂	0.7	0.12
BP	1.13	-0.46
InAs	0.94	0.35

TABLE IV: Parameters L_1 and L_2 for WSe₂, BP, and InAs. After substituting W_D , λ , E_g , and m^* , $\Lambda\sqrt{m^*E_g}$ can be rearranged as

$$\Lambda\sqrt{m^*E_g} = (\lambda + W_D)\sqrt{m^*E_g}$$

$$= \left(L_1T_{ch} + L_2 + \frac{\pi(\varepsilon_1T_{ch} + \varepsilon_2) \left(E_{g,bulk} + \frac{\alpha}{T_{ch}} \right)}{\ln(4)qNT_{ch}} \right) \sqrt{m^* \left(E_{g,bulk} + \frac{\alpha}{T_{ch}} \right)}$$

$$= \left(c_0T_{ch} + c_1 + c_2\frac{1}{T_{ch}} + c_3\frac{1}{T_{ch}^2} \right) c_4\sqrt{1 + c_5\frac{1}{T_{ch}}} \quad (15)$$

where c_1 to c_5 are

$$c_0 = L_1 \quad (16)$$

$$c_1 = L_2 + \beta_1E_{g,bulk} \quad (17)$$

$$c_2 = \beta_2E_{g,bulk} + \beta_1\alpha \quad (18)$$

$$c_3 = \beta_2\alpha \quad (19)$$

$$c_4 = \sqrt{m^*E_{g,bulk}} \quad (20)$$

$$c_5 = \frac{\alpha}{E_{g,bulk}} \quad (21)$$

$$\beta_1 = \frac{\pi\varepsilon_1}{\ln(4)qN} \quad (22)$$

$$\beta_2 = \frac{\pi\varepsilon_2}{\ln(4)qN} \quad (23)$$

c_1 to c_5 for the three channel materials are listed in the Table V.

channel	c_0	c_1	c_2	c_3	c_4	c_5	β_1	β_2
WSe ₂	0.7	1.78	0.85	0.01	0.554	0.01	1.24	0.54
BP	1.14	-0.24	0.71	0.57	0.12	1.79	0.78	1.14
InAs	0.94	0.91	2.77	1.56	0.09	4.28	1.60	1.04

TABLE V: Parameters c_1 to c_5 for WSe₂, BP, and InAs.

REFERENCES

- [1] M. Bohr, "Intels Revolutionary 22 nm Transistor Technology." http://download.intel.com/newsroom/kits/22nm/pdfs/22nm-Details_Presentation.pdf, 2011. [Online].

- [2] "International Technology Roadmap for Semiconductors (ITRS)." <http://www.itrs2.net/>, 2015. [Online].
- [3] R. Gonzalez, B. Gordon, and M. Horowitz, "Supply and threshold voltage scaling for low power CMOS," *IEEE Journal of Solid-State Circuits*, vol. 32, no. 8, pp. 1210–1216, 1997.
- [4] J. Appenzeller, Y.-M. Lin, J. Knoch, and P. Avouris, "Band-to-band tunneling in carbon nanotube field-effect transistors," *Phys. Rev. Lett.*, vol. 93, p. 196805, Nov 2004.
- [5] J. Appenzeller, Y. M. Lin, J. Knoch, Z. Chen, and P. Avouris, "Comparing carbon nanotube transistors - the ideal choice: A novel tunneling device design," *IEEE Transactions on Electron Devices*, vol. 52, no. 12, pp. 2568–2576, 2005.
- [6] W. Y. Choi, B.-g. Park, J. D. Lee, and T.-j. K. Liu, "Tunneling field-effect transistors (tfets) with subthreshold swing (ss) less than 60 mv / dec," vol. 28, no. 8, pp. 743–745, 2007.
- [7] A. M. Ionescu and H. Riel, "Tunnel field-effect transistors as energy-efficient electronic switches," *Nature*, vol. 479, no. 7373, pp. 329–337, 2011.
- [8] A. C. Seabaugh and Q. Zhang, "Low-voltage tunnel transistors for beyond CMOS logic," *Proceedings of the IEEE*, vol. 98, no. 12, pp. 2095–2110, 2010.
- [9] U. E. Avci, D. H. Morris, and I. a. Young, "Tunnel field-effect transistors: Prospects and challenges," *IEEE Journal of the Electron Devices Society*, vol. 3, no. 3, pp. 88–95, 2015.
- [10] R. B. Salazar, H. Ilatikhameneh, R. Rahman, G. Klimeck, and J. Appenzeller, "A predictive analytic model for high-performance tunneling field-effect transistors approaching non-equilibrium Green's function simulations," *Journal of Applied Physics*, vol. 118, no. 16, 2015.
- [11] H. Ilatikhameneh, R. B. Salazar, G. Klimeck, R. Rahman, and J. Appenzeller, "From fowler-nordheim to nonequilibrium green's function modeling of tunneling," *IEEE Transactions on Electron Devices*, vol. 63, pp. 2871–2878, July 2016.
- [12] D. Reuter, C. Werner, a. D. Wieck, and S. Petrosyan, "Depletion characteristics of two-dimensional lateral p-n-junctions," *Applied Physics Letters*, vol. 86, no. 16, pp. 1–3, 2005.
- [13] H. Ilatikhameneh, T. Ameen, F. Chen, H. Sahasrabudhe, G. Klimeck, and R. Rahman, "Dramatic Impact of Dimensionality on the Electrostatics of PN Junctions," pp. 1–5, 2017.
- [14] A. Nipane, S. Jayanti, A. Borah, and J. T. Teherani, "Electrostatics of lateral p-n junctions in atomically thin materials," *Journal of Applied Physics*, vol. 122, no. 19, 2017.
- [15] H. Yu, A. Kutana, and B. I. Yakobson, "Carrier Delocalization in Two-Dimensional Coplanar p-n Junctions of Graphene and Metal Dichalcogenides," *Nano Letters*, vol. 16, no. 8, pp. 5032–5036, 2016.
- [16] H. Ilatikhameneh, T. a. Ameen, G. Klimeck, J. Appenzeller, and R. Rahman, "Dielectric engineered tunnel field-effect transistor," *IEEE Electron Device Letters*, vol. 36, no. 10, pp. 1097–1100, 2015.
- [17] H. Ilatikhameneh, G. Klimeck, J. Appenzeller, and R. Rahman, "Scaling theory of electrically doped 2d transistors," *IEEE Electron Device Letters*, vol. 36, no. 7, pp. 726–728, 2015.
- [18] H. Ilatikhameneh, T. Ameen, B. Novakovic, Y. Tan, G. Klimeck, and R. Rahman, "Saving Moore's Law Down to 1 nm Channels with Anisotropic Effective Mass," *Scientific Reports*, vol. 6, no. August, pp. 1–6, 2016.
- [19] G. B. Beneventi, E. Gnani, A. Gnudi, S. Reggiani, and G. Bacarani, "Dual-metal-gate InAs tunnel FET with enhanced turn-on steepness and high on-current," *IEEE Transactions on Electron Devices*, vol. 61, no. 3, pp. 776–784, 2014.
- [20] T. A. Ameen, H. Ilatikhameneh, G. Klimeck, and R. Rahman, "Few-layer phosphorene: An ideal 2d material for tunnel transistors," *Scientific Reports*, vol. 6, pp. 28515 EP –, Jun 2016. Article.
- [21] A. C. Ford, C. W. Yeung, S. Chuang, H. S. Kim, E. Plis, S. Krishna, C. Hu, and A. Javey, "Ultrathin body InAs tunneling field-effect transistors on Si substrates," *Applied Physics Letters*, vol. 98, no. 11, pp. 98–100, 2011.
- [22] K. Tomioka, M. Yoshimura, and T. Fukui, "Steep-slope tunnel field-effect transistors using III-V nanowire/Si heterojunction," *Digest of Technical Papers - Symposium on VLSI Technology*, no. 2010, pp. 47–48, 2012.
- [23] D. Cutaia, K. E. Moselund, H. Schmid, M. Borg, a. Olziersky, and H. Riel, "Complementary III-V heterojunction lateral NW Tunnel FET technology on Si," *Digest of Technical Papers - Symposium on VLSI Technology*, vol. 2016-Sept, no. 619509, pp. 4–5, 2016.
- [24] H. Ilatikhameneh, "Tunnel field-effect transistors in 2-D transition metal dichalcogenide materials," *Ieee J. Explor. Solid State Computat. Devices Circuits*, vol. 1, no. April, pp. 12–18, 2015.
- [25] H. Ilatikhameneh, G. Klimeck, J. Appenzeller, and R. Rahman, "Design rules for high performance tunnel transistors from 2-D materials," *IEEE Journal of the Electron Devices Society*, vol. 4, no. 5, pp. 260–265, 2016.
- [26] Y. Ma, B. Liu, A. Zhang, L. Chen, M. Fathi, C. Shen, A. N. Abbas, M. Ge, M. Mecklenburg, and C. Zhou, "Reversible Semiconducting-to-Metallic Phase Transition in Chemical Vapor Deposition Grown Monolayer WSe_2 and Applications for Devices," *ACS Nano*, vol. 9, no. 7, pp. 7383–7391, 2015.
- [27] J. C. S. Koster and G. F., "Simplified LCAO Methos for periodic potential problem," vol. 94, 1954.
- [28] C. Gong, H. Zhang, W. Wang, L. Colombo, R. M. Wallace, and K. Cho, "Band alignment of two-dimensional transition metal dichalcogenides: Application in tunnel field effect transistors," *Applied Physics Letters*, vol. 103, no. 5, 2013.
- [29] A. Prakash, H. Ilatikhameneh, P. Wu, and J. Appenzeller, "Understanding contact gating in Schottky barrier transistors from 2D channels," *Scientific Reports*, vol. 7, no. 1, pp. 1–30, 2017.
- [30] K. Novoselov, a. Mishchenko, a. Carvalho, and a. H. Castro Neto, "2d materials and van der waals heterostructures," *Science*, vol. 353, no. 6298, pp. 1–25, 2016.
- [31] K. C. Wang, T. K. Stanev, D. Valencia, J. Charles, A. Henning, V. K. Sangwan, A. Lahiri, D. Mejia, P. Sarangapani, M. Povolotskiy, A. Afzalian, J. Maassen, G. Klimeck, M. C. Hersam, L. J. Lauhon, N. P. Stern, and T. Kubis, "Control of interlayer physics in 2H transition metal dichalcogenides," *Journal of Applied Physics*, vol. 122, no. 22, 2017.
- [32] B. Hoefflinger, "Itrs 2028international roadmap of semiconductors."
- [33] M. Luisier, A. Schenk, W. Fichtner, and G. Klimeck, "Atomistic simulation of nanowires in the $sp^3d^5s^*$ tight-binding formalism: From boundary conditions to strain calculations," *Phys. Rev. B*, vol. 74, p. 205323, Nov 2006.
- [34] V. Wang, Y. Kawazoe, and W. T. Geng, "Native point defects in few-layer phosphorene," *Physical Review B - Condensed Matter and Materials Physics*, vol. 91, no. 4, pp. 1–9, 2015.
- [35] A. Kumar and P. K. Ahluwalia, "Tunable dielectric response of transition metals dichalcogenides MX₂ (M=Mo, W; X=S, Se, Te): Effect of quantum confinement," *Physica B: Condensed Matter*, vol. 407, no. 24, pp. 4627–4634, 2012.
- [36] S. Steiger, M. Povolotskiy, H. H. Park, T. Kubis, and G. Klimeck, "NEMO5: A parallel multiscale nanoelectronics modeling tool," *IEEE Transactions on Nanotechnology*, vol. 10, no. 6, pp. 1464–1474, 2011.
- [37] J. E. Fonseca, T. Kubis, M. Povolotskiy, B. Novakovic, a. Ajoy, G. Hegde, H. Ilatikhameneh, Z. Jiang, P. Sengupta, Y. Tan, and G. Klimeck, "Efficient and realistic device modeling from atomic detail to the nanoscale," *Journal of Computational Electronics*, vol. 12, no. 4, pp. 592–600, 2013.
- [38] H. Ilatikhameneh, T. A. Ameen, C. Chen, G. Klimeck, and R. Rahman, "Sensitivity challenge of steep transistors," *IEEE Transactions on Electron Devices*, vol. 65, pp. 1633–1639, April 2018.